RMS VELOCITY ESTIMATION IN LATERALLY VARYING MEDIA

Walt Lynn

Introduction

Conventional velocity estimation techniques are based on coherency measurements along hyperbolic moveout trajectories defined by v_{rms} [e.g. Taner and Koehler, 1969]. However, the normal moveout is sensitive not only to the rms velocity, but also to its second derivative beneath each midpoint. Where the earth is laterally homogeneous, the effect of the second derivative is zero and is usually ignored even in areas of lateral variation. Thus, in regions of lateral inhomogeneity, the rms velocities obtained by conventional techniques often imply absurd interval velocities.

In this paper we will develop two schemes which incorporate the second lateral derivative into the velocity estimation. The first works on common offset sections and the second on common midpoint slant stacks. The latter is simply a linear moveout and sum of common midpoint (cmp) gathers and has the advantage of better signal to noise properties. We will discuss both the derivation and implementation of these techniques and compare their results with velocity estimations from a conventional semblance technique. Before discussing these, however, we will first examine a set of synthetic cmp gathers over a lateral velocity change to see why conventional techniques breakdown.

An example of why conventional velocity estimation techniques fail in laterally varying media.

To demonstrate the effects of lateral velocity variations on measuring v_{rms} we will consider the model shown in Figure 1. This is essentially the same model used by Pollet (1975) and consists of horizontal beds extending across the entire section with the exception of a 200 foot low velocity layer (5400 ft/sec) which begins at y = 10000 and continues to the right of the model. Synthetic seismograms were generated using a ray tracing program to form a suite of 91 2400% cmp gathers. The midpoint spacing and the offset interval are both equal to 100 ft.

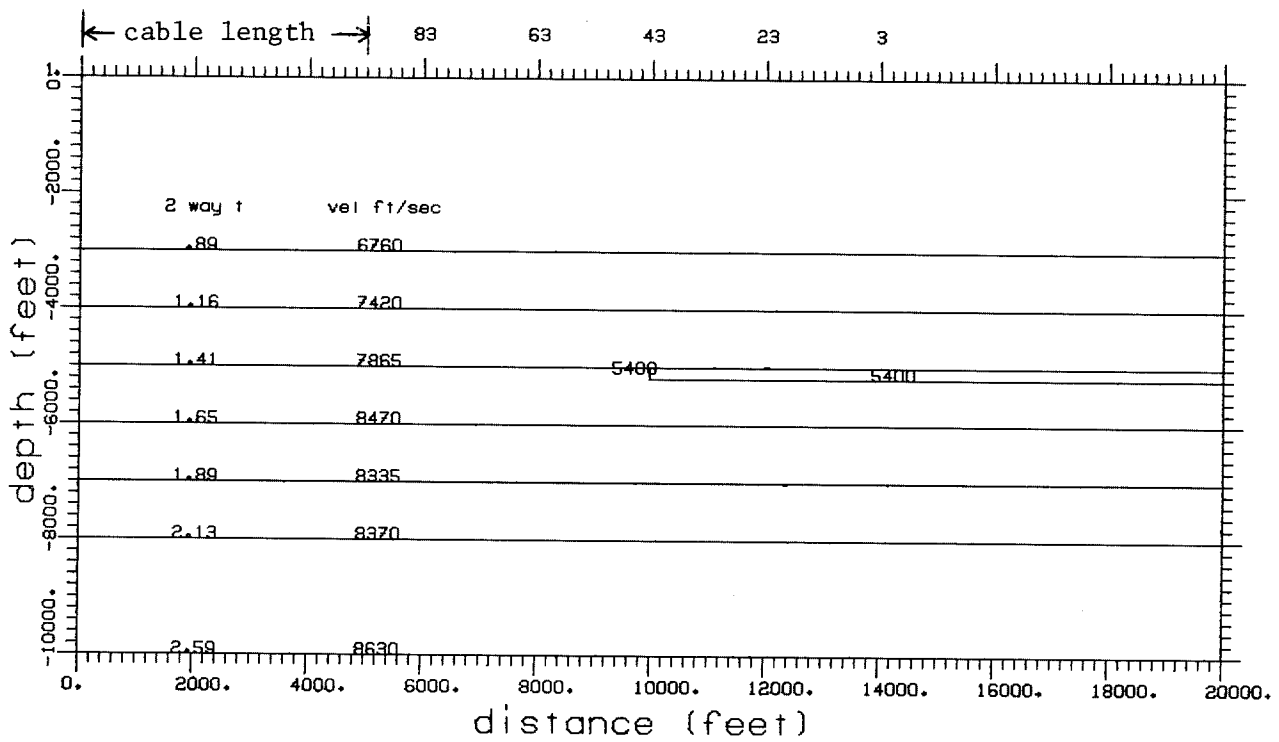

Figure 1 Model used to generate synthetic seismograms for velocity estimation. A total of 91 cmp gathers (#'s 1-91) were generated using a ray tracing program with locations shown at the top of the figure. The cmp gathers are 24 fold with a midpoint and group spacing of 100 ft. Distance to the far offset is 5000 ft. The synthetic traces consist of 3 sec. of 4 msec data. The two-way vertical travel time to the reflectors outside of the low velocity layer are given on the left. Notice the discontinuity occurs at cmp #43. cmp #'s 30, 35,..., 55 are shown in Figure 2.

Figure 2 shows several different cmp gathers along the profile. To examine the effect of the truncated bed consider the event arriving at approximately 2.14 seconds (corresponding to the interface at 8000 ft. in Figure 1). On cmp #30 the event is hyperbolic because all of the raypaths travel through the low velocity layer. Similarly, for cmp #55 the event is hyperbolic because all of the raypaths for this gather miss the low velocity layer. As the midpoint location moves from #30 to #35, the downgoing part of the raypaths (assuming the shots are to the left of the receivers) for the far traces miss the low velocity layer and the total moveout is reduced. Consequently, the velocity estimate obtained by using a coherency measure will be erroneously high [see Figure 3c]. The same is true at cmp #40 where only the inner traces still travel through the low velocity layer on both their downward and upward paths. At cmp #45, the opposite is true, only the inner traces completely miss the low velocity layer and consequently the velocity measured will be erroneously low because of the effective increase in moveout. cmp #50 has all but its far offsets missing the low velocity layer and thus also shows a greater amount of moveout than predicted by the true v_{rms} .

The semblances measured for velocities ranging from 6000 to 10000 ft/sec at $t_o = 1.66$, 1.90, 2.14, and 2.60 and corresponding to the events located at depths of 6000, 7000, 8000, and 10000 feet respectively are shown in Figure 3. The white line connects the semblance maximums and represents the velocity picks to these events. The effect of the truncated bed is readily apparent in the large fluctuations in the velocity estimations. One disconcerting observation is that the adverse effects of the lateral velocity discontinuity increase with t_o , not diminish.

One possible means of reducing the velocity fluctuations, as discussed by Pollet (1975), is to smooth the velocity function by performing a lateral average on the velocities. The results from one such smoothing operator are shown in Figure 4. The light line in each figure is the original estimated velocity (corresponding to the white line in Figure 3) and the heavy line is a smoothed version of it. In this example, 8 adjacent velocity functions were averaged together followed by an averaging of 5 adjacent smoothed velocity funtions. The smoothing did a good job of removing the short wavelength velocity variations for $t_o = 1.66$, but not so good for

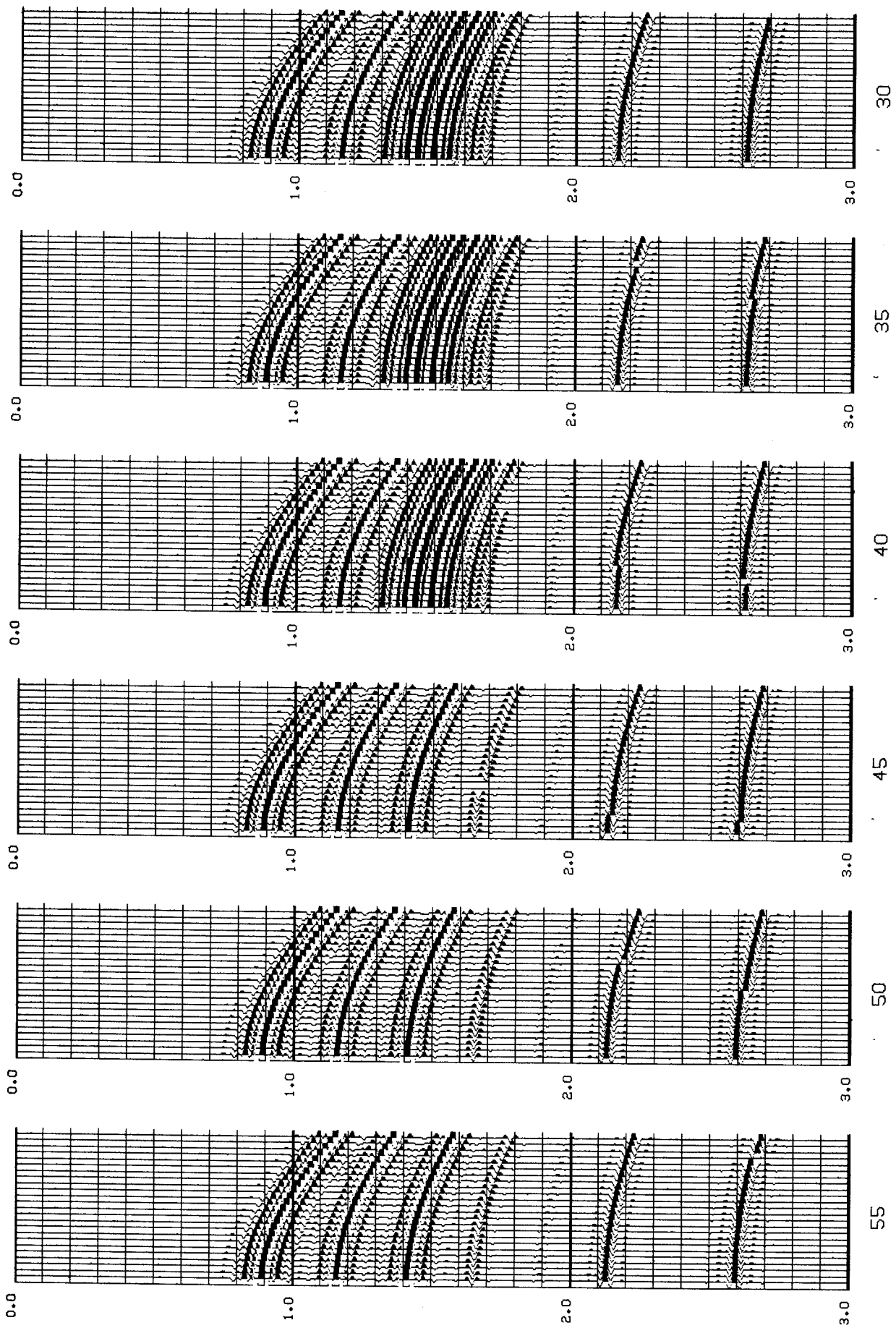

Figure 2. cmp gathers generated using a ray tracing program with the model in Figure 1. Midpoints 30, 35, and 40 are to the right of the discontinuity and 45, 50, and 55 are to the left.

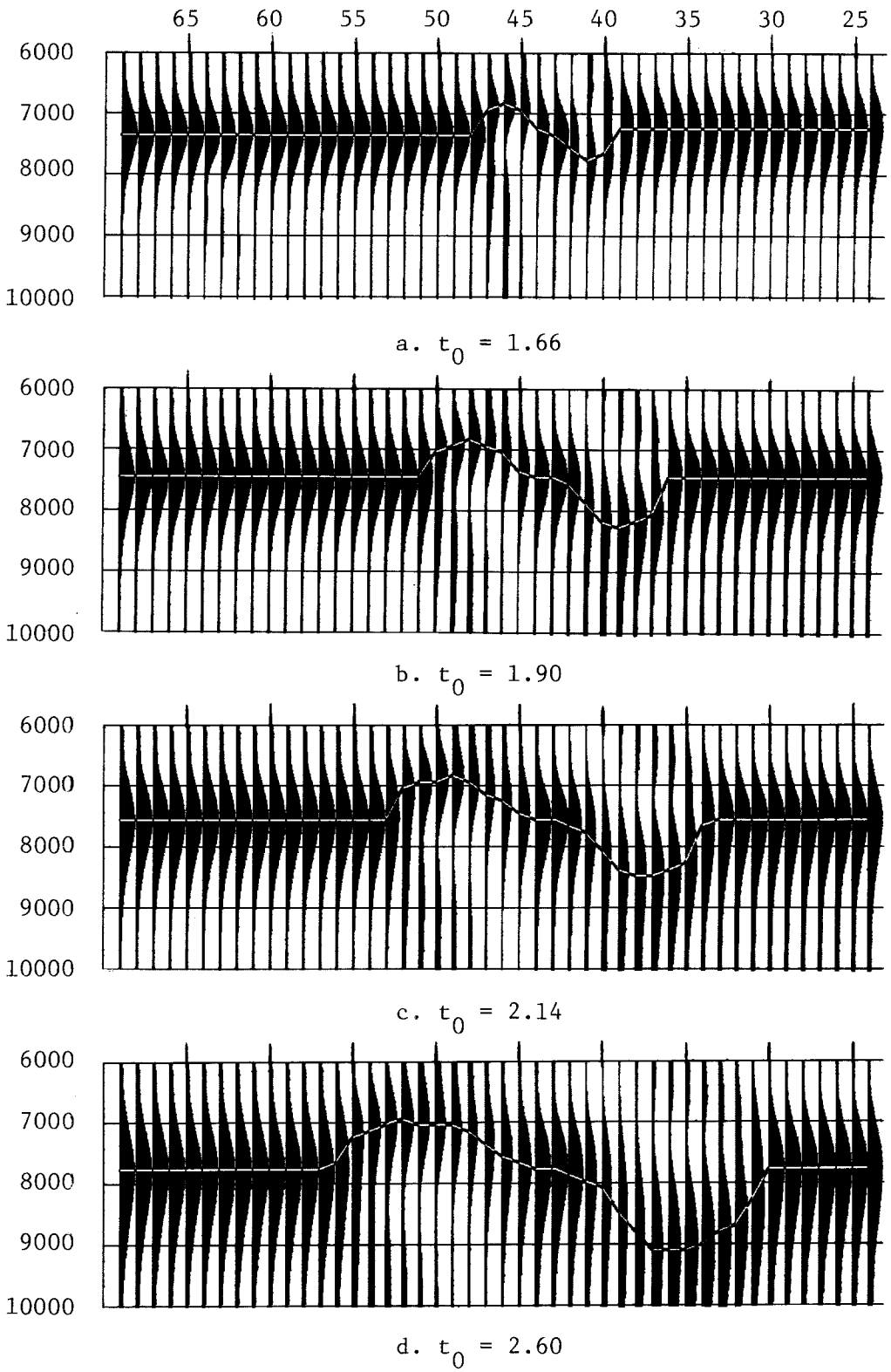

Figure 3. Velocity semblance measures on cmp's #24-69. The low velocity zone discontinuity occurs at cmp #43 and its effect is seen as causing fluctuations in the velocity estimates. Ideally, the rms velocity should change abruptly at cmp #43, being slightly lower on the right. The white line connects the semblance maximum for each midpoint and represents the velocity function one would pick across the section. t_o is the vertical 2-way travel time. The t_o's shown correspond to the interfaces at z = 6000, 7000, 8000, and 10000 feet in Figure 1. Note the effect on the discontinuity increases with t_o.

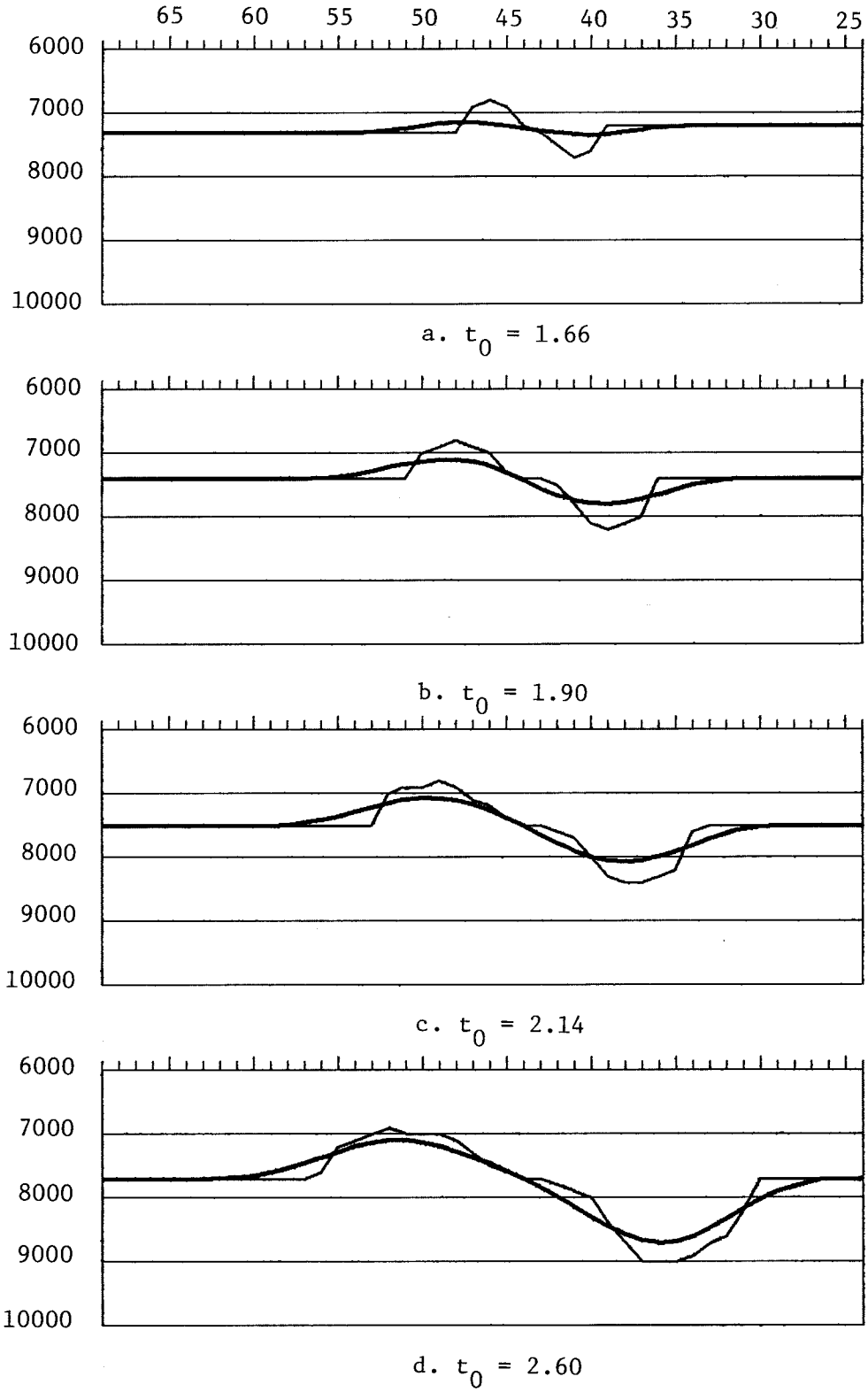

Figure 4. Smoothed version of the velocity curves in Figure 3. The light line in each figure corresponds to the maximum semblance line in Figure 3, the heavy line is a smoothed version. Smoothing was done by averaging 8 adjacent velocities followed by an averaging of 5 adjacent smoothed velocities. Only the velocity for t_o = 1.66 appears to be reasonable. The later t_o's would require much more smoothing to remove the large fluctuations. The problem is, however, how does one know when enough or too much smoothing has been done?

the later times. In fact, in order to smooth the curve at $t_o = 2.60$ sec., we would have to average perhaps 80 - 100 adjacent midpoints.

Clearly there is a lot of subjectivity to smoothing. How can we tell when we have smoothed enough, or too much? Moreover, how can we tell what effects are due to structure and what are artifacts of the velocity estimation procedure? In the next section we will see how to attack this problem by including the effect of the second derivative of the velocity at each midpoint in the velocity estimation.

rms velocity estimation in a laterally varying media using common offset sections

The travel time to a given offset is dependent not only upon the velocity beneath the midpoint but is also dependent upon the lateral derivatives of the velocity. The most important of these is the second lateral derivative. We will now develop a theory which incorporates the effect of this derivative into the velocity estimation. The theory can be applied to either constant offset sections or common midpoint slant stacks. This section will discuss the application for the common offset case. In the following section we will extend the method to work on common midpoint slant stacks where the signal to noise properties are better.

Consider the model in Figure 5 where the velocity above the horizontal reflector at depth z varies in the midpoint (y) direction.

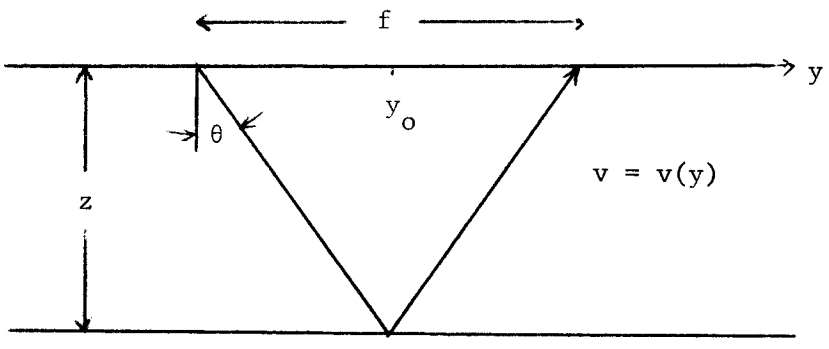

Figure 5

To a first (straight ray) approximation, the travel time to a given offset f is

$$t \cong \int_{-f/2}^{f/2} \frac{w(y)\, dy}{\sin \theta} \quad ,$$

where θ is the angle between the ray and the vertical and $w(y) = 1/v(y)$ is the slowness. Expanding $w(y)$ in a second order Taylor series about $y = y_o$

$$t \cong \frac{1}{\sin \theta} \int_{-f/2}^{f/2} (w_o + y w_o' + \frac{y^2}{2} w_o'') \, dy \quad ,$$

which gives

$$t \cong \frac{1}{\sin \theta} [f w_o + (f^3/24) w_o''] \quad ,$$

or

$$t \cong (f^2 + 4z^2)^{1/2} [w_o + (f^2/24) w_o''] \quad . \qquad (1)$$

Thus, to a first approximation the travel time t is independent of the horizontal gradient, w', but does depend upon the second derivative w'' as well as w_o. If $w'' = 0$, equation (1) reduces to the familar hyperbolic travel time formula

$$t = [(f w_o)^2 + (2z w_o)^2]^{1/2} = [(f/v_o)^2 + t_o^2]^{1/2} \quad .$$

Writing equation (1) in finite difference form using the (1, -2, 1) second derivative operator, it becomes

$$t_j = (f^2 + 4z^2)^{1/2} [a w_{j-1} + (1-2a) w_j + a w_{j+1}] \quad , \; j=1,2,\ldots,N, \qquad (2)$$

where $a = f^2/24\Delta y^2$.

Equation (2) represents a tri-diagonal system of N equations for N midpoints which can be quickly solved to yield w(y). t_j is the travel time to a given fixed offset, f, for the raypaths reflecting off a horizontal reflector at some depth z. Δy is the midpoint spacing. The unattractive feature in the equation is the presence of the variable z , the reflector depth. We will temporarily take z to be known. Later we will show how it can be estimated and improved upon in an iterative manner.

If we had noise free data, we would have no problems with using $w'' \tilde{=} (w_{j-1} - 2w_j + w_{j+1})/\Delta y^2$ as our estimate to the second derivative of the slowness. Since we do not, we will use instead

$$w'' \tilde{=} (w_{j-k} - 2w_j + w_{j+k})/(k\Delta y)^2,$$

where k is some integer number of midpoints greater than 1. The parameter k can be considered as a stability factor. In our tests so far we have chosen it to equal the number of midpoints within 1/4 the offset, i.e. $k\Delta y = f/4$ [see Figure 6]. Because we are not using the adjacent midpoints in estimating the second derivative of the slowness, w" , but rather those at $\pm$ 1/4 f , we are imposing the restriction that the second derivative be constant over 1/2 the offset used.

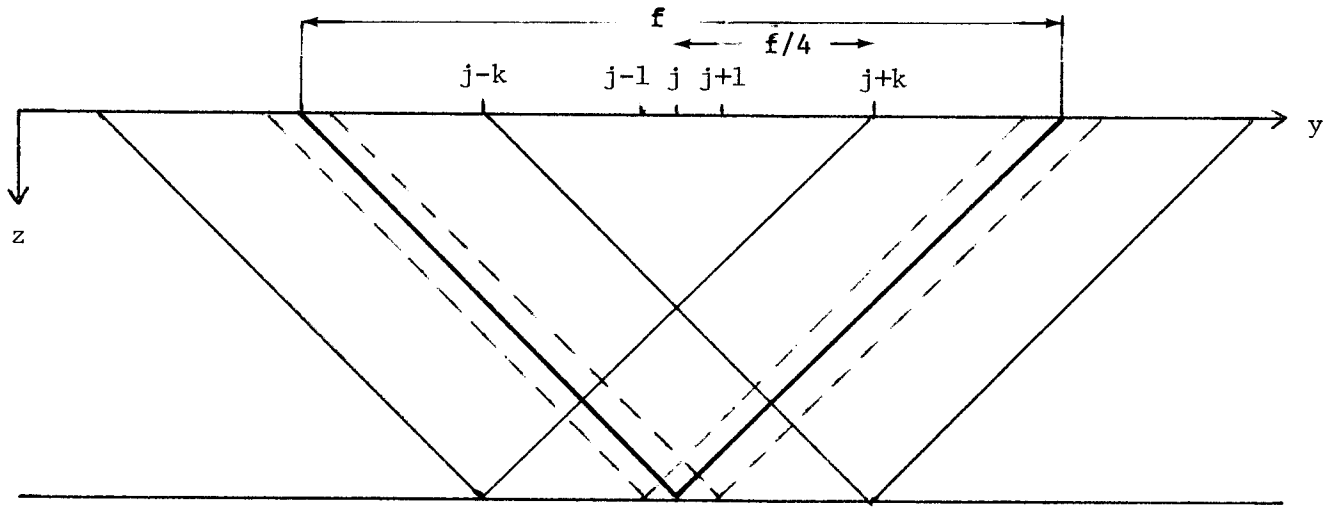

Figure 6. Raypaths to the offset f for the midpoints j-k, j-1, j, j+1, and j+k. k is chosen to be $f/4\Delta y$, where Δy is the midpoint spacing.

Using the above approximation for w'' , equation (2) becomes

$$t_j = (f^2 + 4z^2)^{1/2} \left[a'w_{j-k} + (1-2a')w_j + a'w_{j+k}\right] , \qquad (3)$$

where $a' = f^2/(24k^2\Delta y^2)$.

In matrix form, equation (3) looks like

$$\begin{bmatrix} d & 0 & c & & & & & & & & \\ 0 & d & & c & & & & & & & \\ c & & d & & c & & & & & & \\ & c & & d & & c & & & & & \\ & & c & & d & & c & & & & \\ & & & c & & d & & c & & & \\ & & & & c & & d & & c & & \\ & & & 0 & & c & & d & & c & \\ & & & & & & c & & d & & \\ & & & & & & & c & & d & \\ & & & & & & & & c & & d \end{bmatrix} \begin{bmatrix} \\ \\ \\ \\ \\ \\ \\ \\ \\ \\ \\ \end{bmatrix} \overline{w} = \begin{bmatrix} \\ \\ \\ \\ \\ \\ \\ \\ \\ \\ \\ \end{bmatrix} \overline{t} \qquad (4)$$

where $c = a'(f^2 + 4z^2)^{1/2}$ and $d = (1-2a')(f^2 + 4z^2)^{1/2}$. The number of zero diagonals between the main diagonal and the non-zero diagonals is $k-1$. This system of equations decouples into k independent tri-diagonal systems of equations

$$\begin{bmatrix} d & c & & & & & & & & & \\ c & d & c & & & & & & & & \\ & c & d & c & & & & & & & \\ & & c & d & c & & & & & & \\ & & & c & d & c & & & & & \\ & & & & c & d & c & & & & \\ & & & 0 & & c & d & c & & & \\ & & & & & & c & d & c & & \\ & & & & & & & c & d & c & \\ & & & & & & & & c & d & c \\ & & & & & & & & & c & d \end{bmatrix} \begin{bmatrix} w_i \\ w_{i+k} \\ w_{i+2k} \\ \vdots \\ \\ \\ \\ \\ \\ \\ \\ \end{bmatrix} = \begin{bmatrix} t_i \\ t_{i+k} \\ t_{i+2k} \\ \vdots \\ \\ \\ \\ \\ \\ \\ \\ \end{bmatrix} , \; i = 1,2,\ldots,k \qquad (5)$$

and is easily solved. This is the system of equations used to estimate the velocity for the constant offset case.

The constant offset velocity estimation scheme was tested on the synthetic gathers generated using the model in Figure 1. The rms velocities to the four interfaces below the truncated bed are shown in Figure 7 (a-d) as the heavy lines. Superimposed, as a lighter line, are the semblance results seen earlier in Figure 3. The velocities in Figure 7 were computed by first picking the arrival times at the 2000 foot offset. The midpoint spacing is 100 ft. so the parameter k is equal to 5. This gave 5 different sets of equations like equation 5. In order to avoid instability and provide some coupling between the sets of equations, the travel times, t_j, were smoothed over 8 adjacent traces. The number 8 is arbitrary. Averages from 3 to 15 were tried without much change in the result. The known depth to each reflector was inserted into the coefficients c and d in equation (5).

The velocities for the layers at 6000, 7000, and 8000 feet (Figure 7a-c) are remarkably improved over the semblance measures. The fact that there is some ripple in the velocity vs. midpoint curves is probably due to the fact that the synthetic data does not satisfy the assumptions of our model very well. That is, the velocity can not be accurately expressed at each midpoint as a second order Taylor's series. The velocity to the layer at 10000 feet is poor for the same reason.

The solution to equation (5) involves a knowledge about the depth z to the reflector, which in general is not known. We can estimate the depth in several ways. One is to use an average depth computed from t_o, the vertical two-way travel time, and the velocity estimated by doing coherency measures with $z = vt_o/2$. However, to avoid the work of doing coherency measures, we can estimate z by considering 2 different constant offset sections. At a given midpoint the approximate travel time t_j to an offset f_j is

$$t_j = (f_j^2 + 4z^2)^{1/2}/v_j \quad .$$

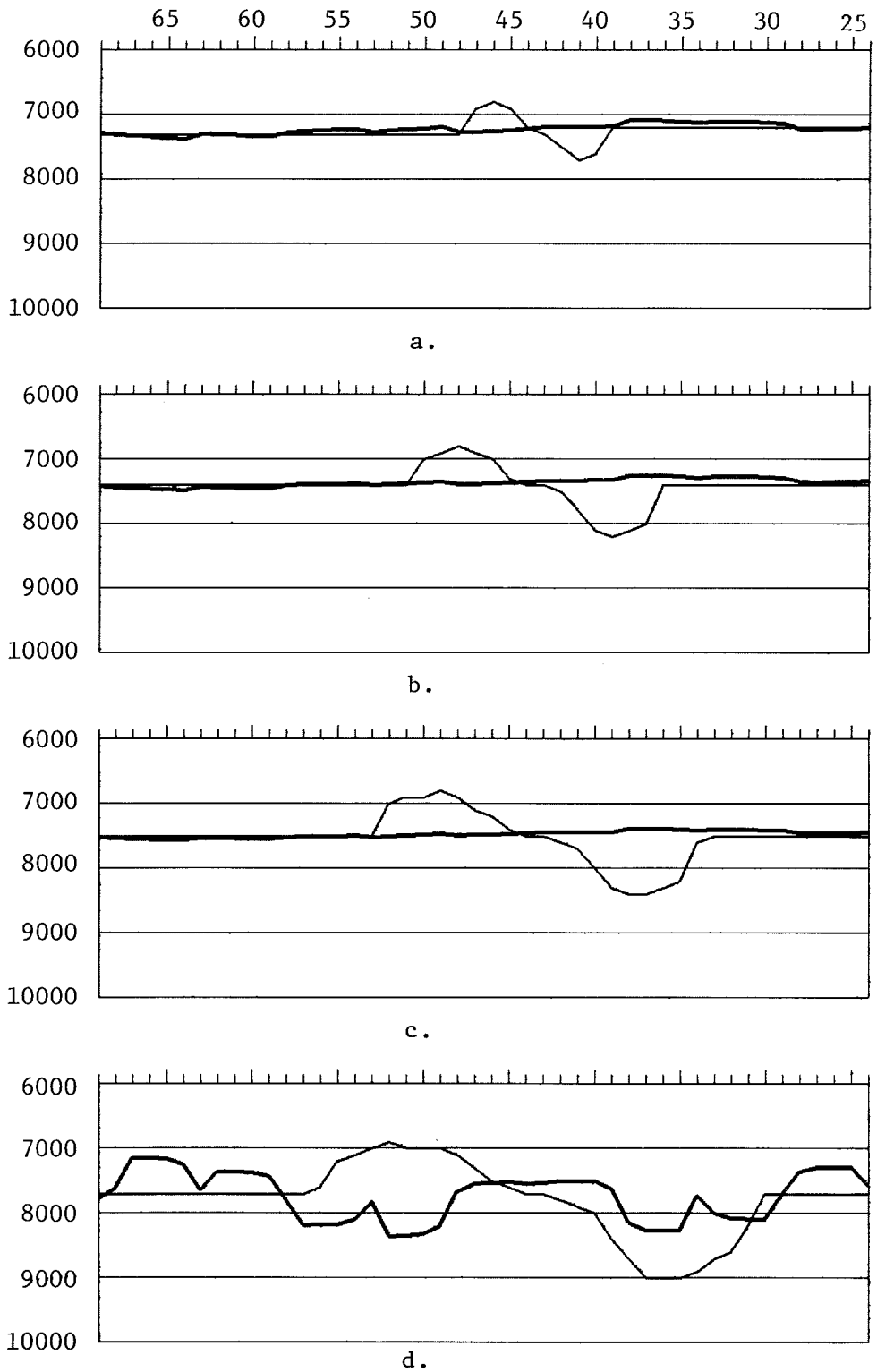

Figure 7. rms velocities to the reflectors in Figure 1 at a) 6000, b) 7000, c) 8000, and d) 10000 feet using equation 5. Light lines are velocities computed using a semblance measure and are the same as the white lines in Figure 3 (a-d). With the exception of d, the estimated rms velocity to these refectors is much improved over the semblance technique. The ripple in the dark curves as well as the failure of the method in d) are due to the fact that the model used to generate the synthetics violates a major assumption of the velocity being accurately expressable at every midpoint in a second order Taylor's series expansion.

Writing this equation for two different offsets and eliminating the velocity we get

$$z = \left(\frac{t_1^2 f_2^2}{t_2^2} - f_1^2 \right) / 4 \left(1 - \frac{t_1^2}{t_2^2} \right).$$

After computing z for each midpoint, an average value can be used in equation (5). The coefficients to the system of equations can then be updated using the computed velocities and a second iteration of velocity estimates can be made. This procedure is continued until convergence of the velocity function.

One very foreseeable problem when applying the constant offset technique to real data is that of poor signal to noise ratios. Reflectors on constant offset sections are often too weak to be picked with any high degree of reliability. Consequently, it would be advantageous to work with some sort of stacked section where the signal to noise ratio is enhanced. In the following section we will extend the method presented above to work on common midpoint slant stacks, that is, a linear moveout and sum of common midpoint gathers.

rms velocity estimation using cmp slant stacks

In this section we will extend the ideas presented in the previous section to estimate velocity using common midpoint slant stacks. These are not to be confused with common shot or common receiver slant stacks which correspond to a specific realizable experiment. A common midpoint slant stack is nothing more than a stacking of cmp gathers along linear moveout trajectories and does not correspond to any sort of realizable experiment. As with common shot and common receiver slant stacks, the main contribution to the stack for each event comes from the Fresnel zone, the region of tangency with the linear moveout trajectory (Figure 8).

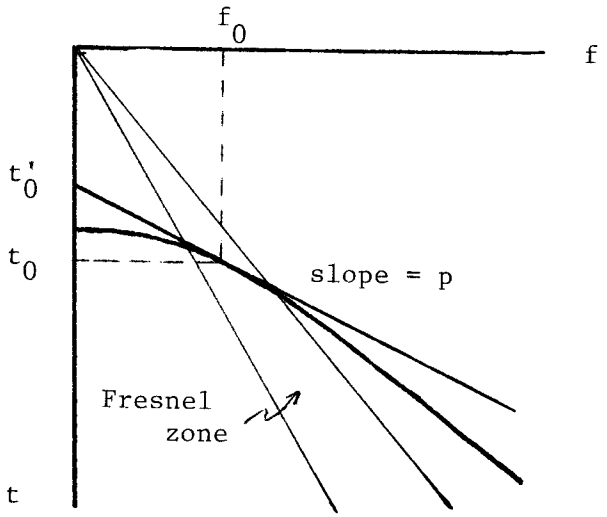

Figure 8 Tangency method of estimating rms velocity. v_{rms} is given by f_o/pt_o or $f_o/p(t'_o + pf_o)$. (see Claerbout (1977)).

The offset at which the Fresnel zone is centered increases with time so common midpoint slant stacks are like a common offset section where the offset increases with time.

The basis of the method to be presented is found in Schultz (1976) and in Claerbout (1977). Referring to Figure 8, the rms velocity is obtained from f_o, t_o, and p , where (f_o,t_o) is the point of tangency of the hyperbolic event with a line of slope p and is given by

$$v^2_{rms} = f_o/pt_o = f_o/p(t'_o + pf_o) \quad . \tag{6}$$

The velocity information is now obtained from a Fresnel zone as opposed to the whole range of offsets as with coherency techniques.

Now consider measuring v_{rms} at several different p values. To a first approximation, the effect is to get the rms velocity along raypaths shown in Figure 9.

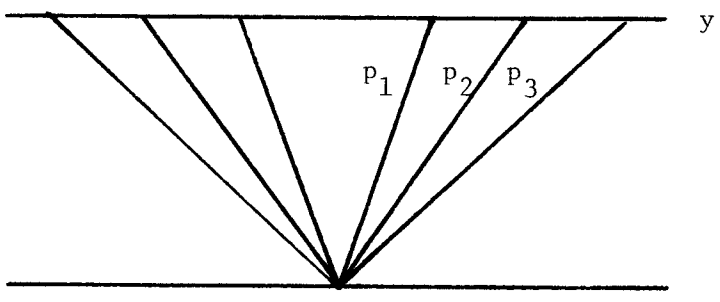

Figure 9 Raypaths for different p values sample different regions below the midpoint.

We can imagine designing an inverse procedure to get the rms velocity for the entire area covered by the raypaths by using the rms velocity information from a range of p values (and hence offsets). Moreover, if we combine this information with all of the other common midpoint gathers we could obtain $v(y)$ for the entire section. This type of approach is very similar to the x-ray tomographic imaging methods used in medicine.

We will consider a much simpler case wherein we will examine only one p value. Recalling equation (1) from the previous section and writing $t' = t - pf$ we have

$$t' \cong \frac{1}{\sin\theta}\left[fw_o + (f^3/24)w_o''\right] - pf \quad . \tag{7}$$

Using $\sin\theta \cong pv_o = p/w_o$ gives

$$t' \cong \frac{fw_o}{p}\left[w_o + (f^2/24)w_o''\right] - pf \quad . \tag{8}$$

The known parameters in equation (8) are t' and p. The former is picked from the slant stack and the latter is a constant for the entire stack. The offset f could be measured by examining each individual common midpoint gather, however, we can estimate it by using equation (6)

$$f_j \cong pv_j^2 t_j = pv_j^2(t_j' + pf_j)$$

or

$$f_j \cong \hat{f}_j = \frac{pv_j^2 t_j'}{1-p^2v_j^2} \quad ,$$

where the subscript j refers to the midpoint number. Equation (8) now becomes

$$t'_j = \frac{w_j \hat{f}_j}{p} \left[w_j + (\hat{f}_j^2/24) w''_j \right] - p\hat{f}_j \quad . \tag{9}$$

Writing equation (9) in finite difference form, we have

$$a_j w_{j-1} + b_j w_j + c_j w_{j+1} = d_j \quad , \tag{10}$$

where

$$a_j = c_j = \frac{w_j \hat{f}_j^2}{24 p \Delta y^2} \quad ,$$

$$b_j = \frac{w_j \hat{f}_j}{p} \left(1 - \frac{\hat{f}_j^2}{12 \Delta y^2} \right) ,$$

and

$$d_j = t'_j + p\hat{f}_j \quad .$$

Equation (10) is analogous to equation (2) in the previous section and its implementation proceeds in much the same manner. Since it is non-linear in velocity it must be solved in an iterative manner. As in the constant offset case, we can not depend on enough resolution from t' to approximate w" using adjacent midpoints. Instead, we use the approximation $w'' = w_{j-k} - 2w_j + w_{j+k}$, where k is an integer greater than 1. As before, k can be considered as stability parameter which attempts to suppress the effect of noise in estimating the second derivative. To determine what it should be, we use equation (6) along with the initial estimates of v_{rms} to an event at each midpoint to obtain an average offset f_{ave} . We then take k to be the number of midpoints contained within 1/4 f_{ave} . Again, the 1/4 is arbitrary.

Writing equation (10) using the above second derivative operator we obtain k sets of independent tri-diagonal systems of equations like equation (5):

$$\begin{bmatrix} b_i & c_i & & & \\ a_{i+k} & b_{i+k} & c_{i+k} & & \\ & a_{i+2k} & b_{i+2k} & c_{i+2k} & \\ & & \ddots & \ddots & \ddots \end{bmatrix} \begin{bmatrix} w_i \\ w_{i+k} \\ w_{i+2k} \\ \vdots \end{bmatrix} = \begin{bmatrix} d_i \\ d_{i+k} \\ d_{i+2k} \\ \vdots \end{bmatrix} \qquad (11)$$

The coefficients in equation (11) depend on the velocity so it is necessary to have an initial estimate of the velocities to get the procedure started. One means of doing this would be to estimate the tangency offset for each common midpoint gather and apply equation (6). Alternatively, we can estimate the velocity directly be performing two different cmp slant stacks. The latter method is substantially quicker and easier and works as follows.

Schultz (1976) demonstrated that hyperbolic events in offset, time space map into elliptical events in p, t' space. The equation of the ellipse is given by

$$\left(\frac{t'}{t_o}\right)^2 + p^2 v^2 = 1 \quad , \qquad (12)$$

where t_o is the vertical two-way travel time and $t' = t - pf$ (see Figure 10).

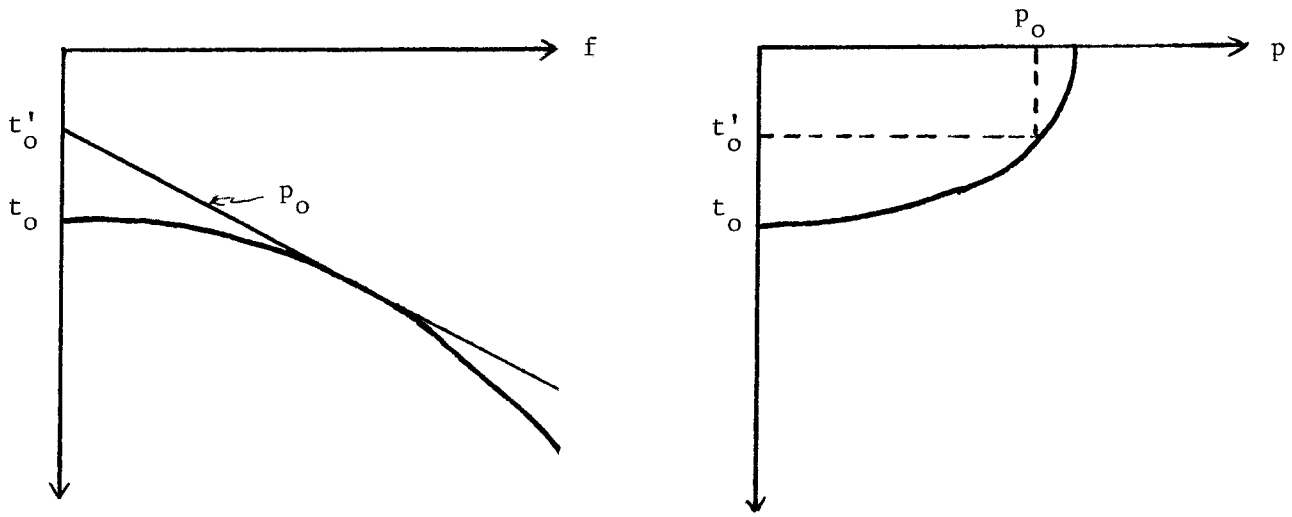

Figure 10 Mapping of hyperbolic events in (f,t) space into elliptical events in (p,t') space.

Knowing t' and p for the same event at the same midpoint for two different slant stacks, we can eliminate t in equation (12) and solve for v_{rms} using

$$v = \frac{1}{p_2}\left[\frac{1 - (t'_2/t'_1)^2}{1 - (p_1 t'_2/p_2 t'_1)^2}\right]^{1/2} . \qquad (13)$$

Figure 11 shows two different common midpoint slant stacks on the synthetic data generated using the model in Figure 1. The stack in Figure 11a was produced by stacking the cmp gathers along a linear trajectory with a slope of $p = 0.0129$ msec/ft. The stack in Figure 11b has $p = 0.0257$ msec/ft. A close up of the events below 1.5 seconds are shown in Figure 12. As an example, consider the event at $\sim$2.1 sec and shown schematically in Figure 13. Measuring t' for this event at each midpoint for the two slant stacks and using equation (13) we obtain the

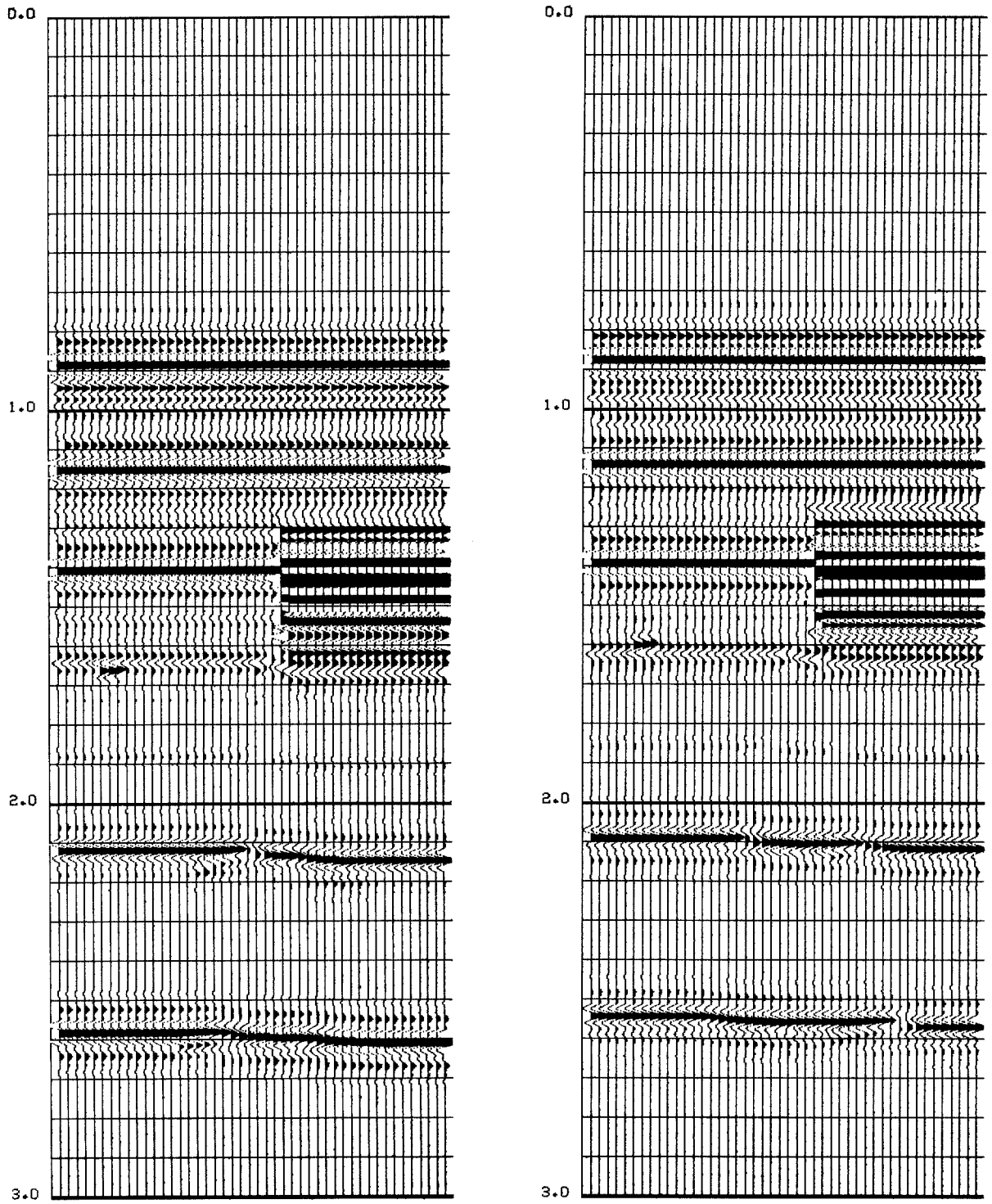

a. b.

Figure 11. Two common midpoint slant stacks of the synthetic data taken from the model in Figure 1. Stacking was done along trajectories defined by $t=t' + pf$, where $p = 0.0129$ and 0.0257 msec/ft in a) and b) respectively. Now windowing or special weighting was done in the stacking. Closeups of the stacks below 1.5 sec. are shown in the next figure.

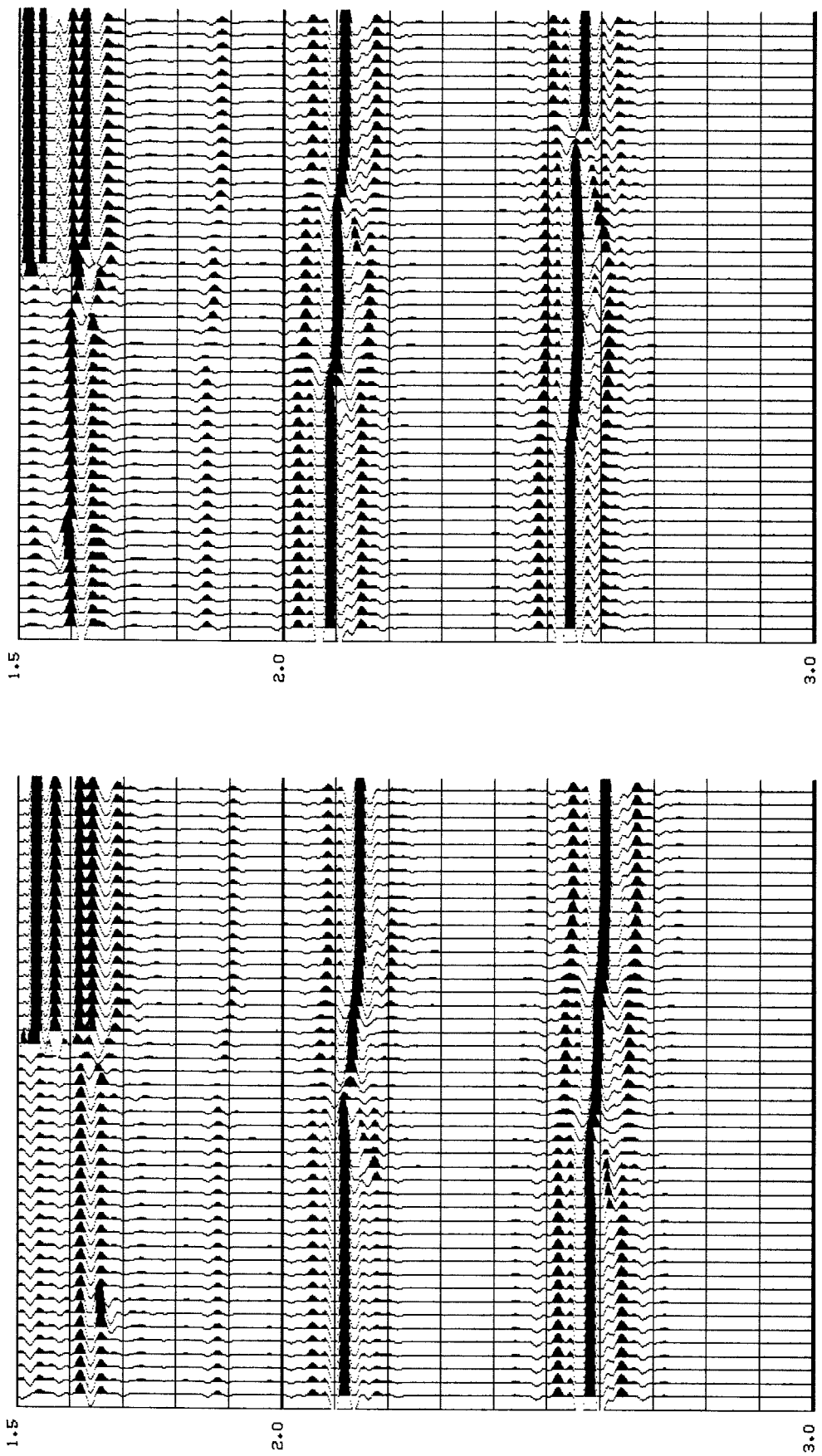

b.

a.

Figure 12. Closeup views of the common midpoint slant stacks in Figure 11. The discontinuity occurs just below 1.5 sec. Note the change in character of the events below the edge of the lateral discontinuity.

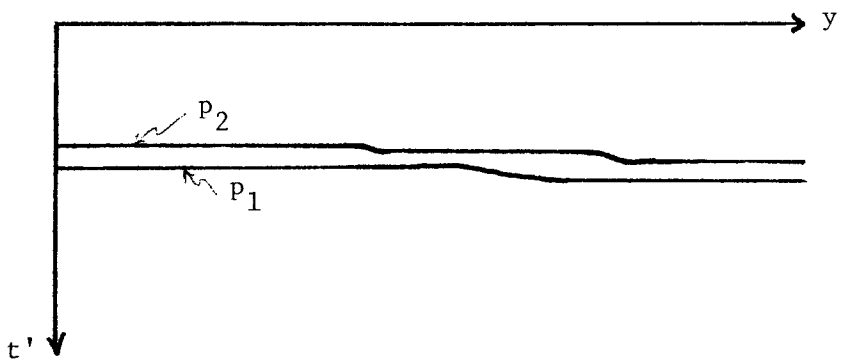

Figure 13. How to measure v_{rms} from two slant stacks. t_1' and t_2' are measured to a given event at the same midpoint for two different slant stacks. These, along with p_1 and p_2, are inserted into equation (13) to obtain v_{rms}.

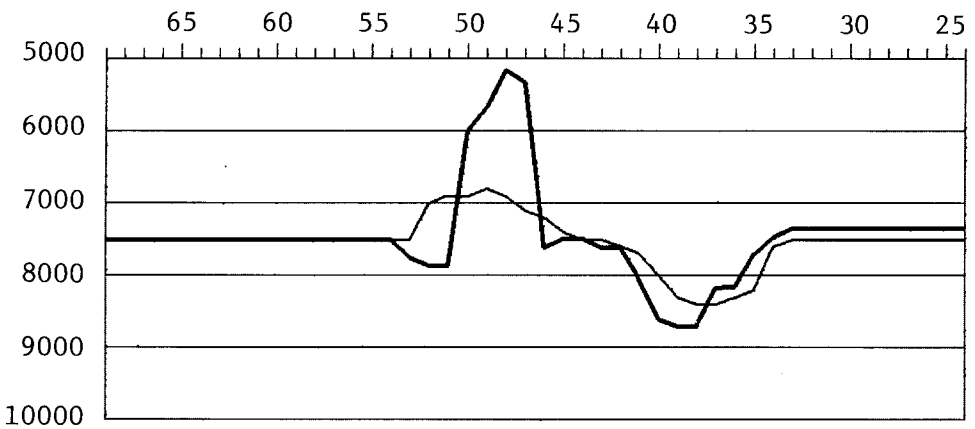

Figure 14. Results from computing an initial velocity estimate to the event at 8000 ft. in Figure 1 using equation (13) (dark line). Velocity estimates computed using a semblance technique are shown as the light line.

rms velocity estimates shown in Figure 14. The results are shown as the dark line and are very similar to the semblance results in Figure 3c. The velocity estimation using the two slant stacks is poorer, but that is to be expected as only two data points are used to determine the velocity as opposed to 24 in the semblance method.

Theoretically, we expect this technique to yield more satisfying results than the constant offset technique because of the better signal to noise properties of the stack. Unfortunately, at this time we have no results using this technique because of some instability problems.

Conclusions

Normal moveout to a event is sensitive to both the rms velocity and the second lateral derivative of the velocity beneath the midpoint. Where the earth is laterally homogeneous, the effect of the latter term is negligible and is usually ignored even in areas of lateral variation. At midpoints where this term is significant, absurd interval velocities can be explained if the second lateral derivative has been ignored.

In this paper we have developed a theory which successfully accounts for both the rms velocity and its second lateral derivative beneath each midpoint. The effect of the first derivative is negligible. The velocity estimation procedure works with either two common offset sections or two common midpoint slant stacks.

The results in Figure 7 from the constant offset scheme are remarkably good. Only on the deepest reflector does the method give poor results. This is due to the poor approximation of the velocity as a second order Taylor's series. This is of no large consequence as we can downward continue the experiment below the low velocity layer using the velocities obtained for the events directly below the truncated bed. The velocity to the interfaces below can then be reestimated with the effect of the low velocity layer removed.

References

[1] Claerbout, J., "How to Measure rms Velocity With a Pencil and Straightedge," SEP 11, (1977), pp. 41-44.

[2] Pollet, Arthur, "Continuous Velocity as an Aid to Hydrocarbon Recognition," Paper presented at the Offshore Technology Conference, (1975), OTC 2271.

[3] Schultz, P., "Velocity Estimation by Wavefront Synthesis," Ph.D. thesis, (1976), Stanford University, Stanford, CA., SEP 9.

[4] Taner, M. and Keohler, F., "Velocity Spectra - Digital Computer Derivation and Applications of Velocity," *Geophysics*, (1969), v. 34, n. 6, pp. 859-881.

[5] Wiggins, R. A., Larner, K. L., and Wisecup, R. D., "Residual Statics Analysis as a General Linear Inverse Problem," *Geophysics*, (1976), v. 41, n. 5, pp. 922-938.